# Proton-neutron multiplet states in $^{112}$Sb

M. Fayez-Hassan, J. Gulyás, Zs. Dombrádi, I. Dankó, and Z. Gácsi
*Institute of Nuclear Research, 4001 Debrecen, P.O.B. 51, Hungary*
(Received 6 December 1996)

Excited states of $^{112}$Sb were investigated through the $^{112}$Sn$(p,n\gamma)^{112}$Sb reaction. $\gamma$-ray, $\gamma\gamma$-coincidence, and internal conversion electron spectra were measured with Ge(HP) $\gamma$ and superconducting magnetic lens plus Si(Li) electron spectrometers at 8.5, 8.9, 9.1, and 9.3 MeV bombarding proton energies. A significantly extended level scheme was constructed. Spins and parities have been assigned to the levels from Hauser-Feshbach analysis of reaction cross sections, internal conversion coefficients, angular distribution of the $\gamma$ rays, and decay properties of the states. The low lying states were assigned to proton-neutron multiplets on the basis of their decay properties. The energy splitting of these multiplets have been calculated using the parabolic rule. [S0556-2813(97)02505-3]

PACS number(s): 23.20.Lv, 23.20.En, 27.60.+j, 25.40.Kv

## I. INTRODUCTION

The results of our experimental study of odd-odd $^{114-118}$Sb nuclei [1–4] shed light on the behavior of proton-neutron multiplets in these nuclei. The energy split of these multiplets is expected to change smoothly as a function of mass number. Members of multiplets involving orbits with around 0.5 occupation probability lie within a few tens of keV from each other. Since the ground state of $^{112}$Sb is expected to be a member of such a multiplet, several excited states should be located below about 150 keV energy.

In order to extend our knowledge about the structure of the light, odd-odd Sb nuclei, we have investigated the lightest Sb isotope, $^{112}$Sb that can be reached via light ion reaction.

The structure of $^{112}$Sb nucleus was studied already from $^{112}$Te$\rightarrow^{112}$Sb decay by Wigmans *et al.* [5], and in $(p,n\gamma)$ and $(^3$He,$6n\gamma)$ reactions by Kamermans *et al.* [6]. The spin and half-life of the ground state was studied by Miyano and Gil [7]. Although all the methods of the low spin spectroscopy were already used in these works, because of the relatively poor statistics of these measurements only a dozen gamma rays were placed into the $^{112}$Sb level scheme, and spins were assigned only to a few levels, which definitely is not enough to understand the proton-neutron multiplet structure of this nucleus.

To interpret the data previously available on the level structure of $^{112}$Sb, Van Gunsteren *et al.* [8] used a particle-quasiparticle model. The agreement of their theoretical results with our experimental data is not satisfactory.

## II. EXPERIMENTAL TECHNIQUES

The present experiments have been performed at the Debrecen 103 cm isochronous cyclotron. Self-supporting, 0.5 and 2.5-mg/cm$^2$-thick $^{112}$Sn targets, prepared by an evaporation technique from isotopically enriched to 81% metallic powder were applied. For reliable identification of $\gamma$ rays, we also studied the $^{114,116,117,118,119,120}$Sn$+p$ reactions.

The targets were bombarded with 5–30 nA proton beams in $\gamma$ and 100–300 nA in conversion electron spectroscopic measurements at $E_p$=8.7–9.3 MeV energies. The $\gamma$-ray spectra were detected with 20 and 25 % Ge(HP) detectors, and with a $2000\times13$ mm$^3$ planar Ge(HP) low-energy photon spectrometer (LEPS). The detectors were placed at 90° to the beam direction for energy determination and at 125° for intensity measurements. The energy resolution of the detectors were ~2 keV (at 1332 keV) and ~0.8 keV (at 122 keV), respectively. For energy and efficiency calibration of the $\gamma$ spectrometers $^{133}$Ba and $^{152}$Eu sources were used.

Internal conversion electron spectra were measured with a superconducting magnetic lens spectrometer (SMLS) with Si(Li) detectors [9]. The energy resolution and transmission of the SMLS were ~2.7 keV (at 946 keV) and ~10% (for two detectors), respectively. The background from backscattered electrons was reduced with swept energy window technique in the spectrum of the Si(Li) detector. Further background reduction was achieved by using paddle-wheel-shaped antipositron baffles. For calibration of the spectrometer, $^{133}$Ba, $^{152}$Eu, and $^{207}$Bi sources were used.

The $\gamma$-ray and internal conversion electron intensities were normalized by using the internal conversion coefficients of the strongest $^{114,116}$Sb transitions [1,2], since the target contained 9 and 6 % of $^{114,116}$Sn isotopes, respectively.

The angular distributions of $\gamma$ rays were measured at 9.3 MeV proton bombarding energy at 12 angles with respect to the beam direction ranging from 90° to 145° in 5° steps. The solid angle correction factors were $Q_2$=0.983 and $Q_4$=0.945. For normalization of the spectra, we used the 93-keV $^{116}$Sb and the 644.78-keV $^{113}$Sb $\gamma$ rays, which have isotropic distributions, as the half-life of the 93-keV isomeric level is more than 200 ns [10] and the 644-keV transition originates from a spin 1/2 level [11].

The theoretical angular distributions for different spin combinations were fitted to the experimental data in a least-squares procedure using the computer code ANDIST [12]. The attenuation coefficients $\alpha_2$ and $\alpha_4$ were calculated with the CINDY [13] program. $\gamma$-ray feeding of the levels effects the alignment, which was also considered. The optical potential parameters used in the calculations are given in Sec. IV A.

The effect of the angular distribution of the conversion electrons on the measured internal conversion coefficients was estimated using the $\gamma$-ray angular distribution coeffi-

 © 1997 The American Physical Society

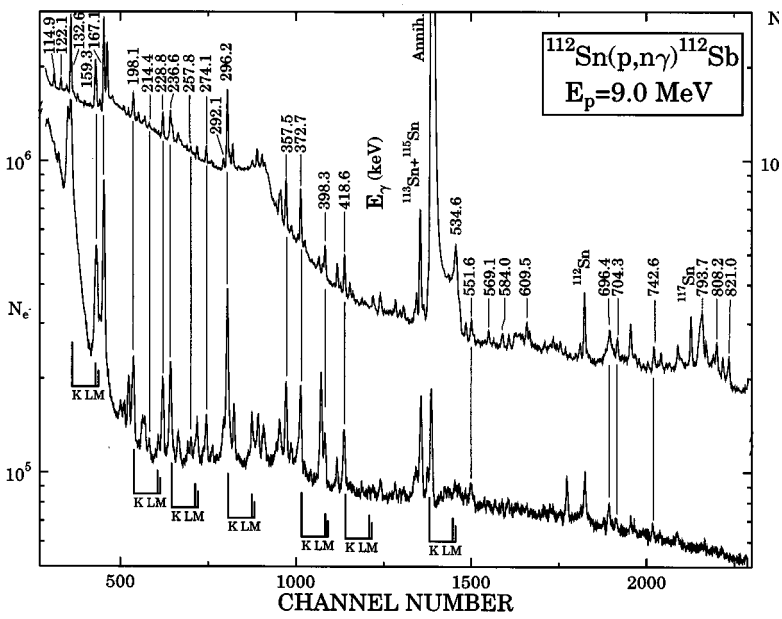


FIG. 1. Typical $\gamma$-ray and internal conversion electron spectra of the $^{112}$Sn$(p,n\gamma)^{112}$Sb reaction. $K$, $L$, $M$ denote conversion electron lines.

cients, the solid angle correction factors and the normalized directional particle parameters. It was found that this effect is much smaller than the statistical uncertainty of the conversion coefficients.

The $\gamma\gamma$-coincidence data were acquired at 9.3 MeV bombarding proton energy, with a fixed $\tau$=80 ns resolving time. The 20 and 25 % Ge(HP) detectors were placed at 125° and 235° angles to the beam direction. Approximately 35 million $\gamma\gamma$-coincidence events were recorded on magnetic tapes in event-by-event mode for subsequent analysis. After creating the symmetrized, two-parameter coincidence matrices, a standard gating procedure was applied.

All measurements were performed with CAMAC modular units connected to a TPA 11/440 computer and to multichannel analyzer cards mounted in personal computers. The data reduction was carried out using a $\gamma$-spectrum analyzing program [14].

## III. EXPERIMENTAL RESULTS

Typical $\gamma$-ray and internal conversion electron spectra are shown in Fig. 1. The $\gamma$-spectrum measurement on the other Sn isotopes and the study of the radioactive decay of the reaction products enabled unambiguous $\gamma$-ray identification in most cases. More than 80 $\gamma$ rays were assigned to $^{112}$Sb, 60 of which are new. Several doublets were resolved in the

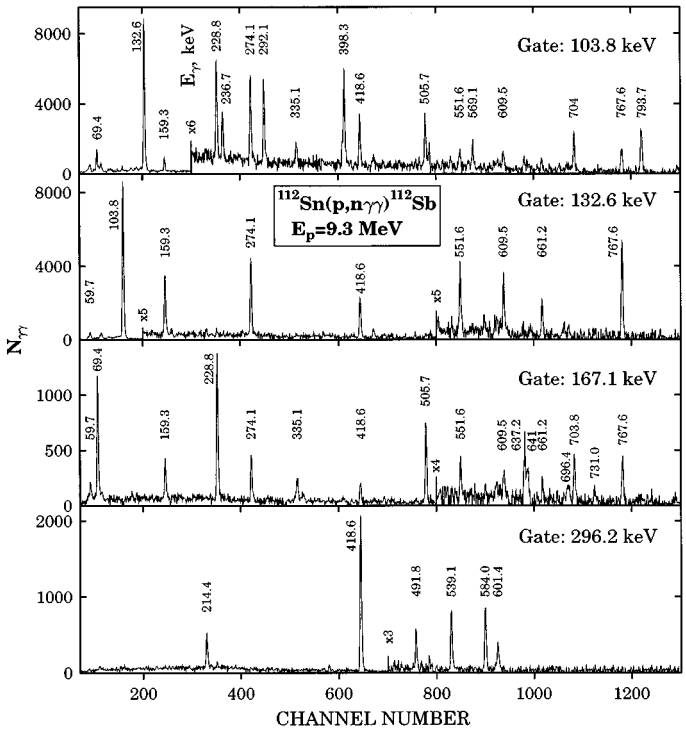


FIG. 2. Typical $\gamma\gamma$-coincidence spectra. The background was subtracted.

TABLE I. The energies, intensities, internal conversion coefficients, multipolarities and coincidence relations of $\gamma$ rays observed in the $^{112}$Sn$(p,n\gamma)^{112}$Sb reaction at $E_p$=9.3 MeV. *N* means new transition.

| $E_\gamma$ (keV) | $I_\gamma$ (relative) | | ICC measurement $10^3\times\alpha_K$ | $\gamma$ multipol. | Coincident $\gamma$ rays (keV) | | | | | |
|---|---|---|---|---|---|---|---|---|---|---|
| 22.7 | | *N* | | | | | | | | |
| 25.8 | | *N* | | | | | | | | |
| 37.5(4) | 28(15) | *N* | | | | | | | | |
| 38.3(4) | 113(60) | | | | | | | | | |
| 59.7(1) | 51(9) | | | | 69 | 104 | 133 | 167 | 198 | 237 |
| | | | | | 419 | | | | | |
| 69.39(4) | 77(15) | | | | 60 | 104 | 159 | 167 | 274 | 419 |
| | | | | | 552 | 609 | 661 | | | |
| 99.9(3) | 7(2) | *N* | | | 296 | | | | | |
| 103.8(1) | 1000(70) | | | | 60 | 69 | 115 | 122 | 133 | 159 |
| | | | | | 214 | 229 | 237 | 274 | 292 | 335 |
| | | | | | (370) | (396) | 398 | 419 | 437 | (450) |
| | | | | | 492 | 472 | 506 | 535 | 539 | 552 |
| | | | | | 569 | (584) | 609 | 637 | 641 | 661 |
| | | | | | 685 | (696) | 704 | (731) | 768 | 794 |
| | | | | | 864 | 874 | | | | |
| 114.9(5) | 42(9) | *N* | | | 104 | 133 | 159 | 167 | 229 | 237 |
| | | | | | 292 | 358 | | | | |
| 122.1(1) | 24(4) | *N* | | | 104 | (641) | 704 | 808 | | |
| 132.59(4) | 351(20) | | 225(44) | *M*1 | 60 | 104 | (115) | 159 | (214) | 274 |
| | | | | | (370) | 419 | 437 | (450) | 492 | 539 |
| | | | | | 551 | (585) | (601) | 609 | 661 | 696 |
| | | | | | 768 | | | | | |
| 159.3(4) | 42(4) | *N* | 158(50) | *M*1,*E*2 | 69 | 104 | (115) | 133 | 167 | 198 |
| | | | | | 237 | 450 | 535 | 696 | | |
| 167.10(4) | 409(21) | | 102(30) | *M*1 | 60 | 69 | (115) | 159 | (214) | 229 |
| | | | | | 274 | 335 | 419 | (436) | (450) | 506 |
| | | | | | 551 | 609 | 637 | 641 | 661 | 696 |
| | | | | | 704 | 731 | 768 | 841 | | |
| 198.08(4) | 110(11) | | 75(14) | *M*1 | 60 | 159 | 274 | 419 | 437 | (552) |
| | | | | | 610 | (661) | | | | |
| 214.4(1) | 28(4) | *N* | 55(8) | *M*1 | 60 | (69) | 104 | 133 | (167) | 296 |
| 228.2(3) | 28(3) | *N* | 50(5) | | 104 | 115 | 167 | 296 | 419 | 450 |
| 228.8(2) | 99(5) | | | | 535 | 696 | | | | |
| 236.6(3) | 60(27) | | 67(18) | | 60 | 104 | 115 | 159 | 274 | 419 |
| 236.7(3) | 39(18) | | | | 437 | 532 | 609 | | | |
| 257.8(1) | 34(4) | *N* | 39(5) | *M*1 | 419 | | | | | |
| 274.05(4) | 88(4) | | 38(4) | *M*1,*E*2 | 69 | 104 | 133 | 167 | 198 | 237 |
| | | | | | (370) | | | | | |
| 279.8(1) | 30(9) | | 51(2) | *M*1,*E*2 | 419 | | | | | |
| 292.1(1) | 46(5) | *N* | 48(2) | *M*1,*E*2 | 104 | (115) | (450) | 696 | | |
| 296.18(4) | 615(23) | | 32(3) | *M*1,*E*2 | 100 | 214 | 228 | 419 | 492 | 539 |
| | | | | | 584 | 601 | 691 | | | |
| 335.1(1) | 45(9) | *N* | 29(9) | *M*1,*E*2 | 104 | 167 | 396 | (471) | | |
| 350.0(4) | 123(18) | *N* | | | 370 | 448 | 458 | 492 | 554 | 598 |
| 357.54(4) | 231(11) | | 17(2) | *M*1,*E*2 | 115 | 450 | 535 | 696 | | |
| 369.8(1) | 38(4) | *N* | 16(2) | | 104 | 133 | 214 | 274 | 350 | 373 |
| 370.2(5) | 8(2) | *N* | | | 511 | | | | | |
| 372.72(4) | 313(8) | | 17(2) | *M*1,*E*2 | 370 | 448 | 458 | 492 | 554 | 598 |
| 377.1(5) | 7(4) | *N* | | | | | | | | |
| 395.9(4) | 33(11) | *N* | 12(1) | *M*1,*E*2 | 104 | (167) | 335 | 398 | | |

TABLE I. (*Continued*).

| $E_\gamma$ (keV) | $I_\gamma$ (relative) | | ICC measurement $10^3\times\alpha_K$ | $\gamma$ multipol. | Coincident $\gamma$ rays (keV) | | | | | |
|---|---|---|---|---|---|---|---|---|---|---|
| 398.25(4) | 75(11) | | 14(2) | $M1,E2$ | 104 | 396 | 472 | | | |
| 418.59(5) | 259(18) | | 12(2) | $M1,E2$ | 60 | 69 | 104 | 133 | 167 | 198 |
| | | | | | 228 | 237 | 258 | 280 | 296 | |
| 436.8(4) | 29(2) | *N* | 12(2) | $M1,E2$ | 104 | 133 | 167 | (198) | 237 | |
| 448.2(1) | 35(5) | *N* | | | 350 | 373 | | | | |
| 450.1(1) | 19(7) | *N* | 10(1) | $M1,E2$ | 104 | 133 | 159 | (167) | 229 | (292) |
| | | | | | 358 | | | | | |
| 458.0(3) | 12(2) | *N* | | | 350 | 373 | | | | |
| 471.8(1) | 33(11) | | 10(2) | $M1,E2$ | 104 | 398 | | | | |
| 491.8(4) | 50(11) | *N* | 8.2(18) | | 104 | 132 | 296 | 350 | 373 | |
| 491.9(2) | 21(7) | *N* | | | | | | | | |
| 505.7(5) | 131(35) | *N* | 7.5(9) | $M1,E2$ | 104 | 167 | | | | |
| 510.7(3) | 174(35) | *N* | | | 370 | | | | | |
| 534.56(9) | 35(7) | *N* | | | 104 | 159 | 167 | 229 | 358 | (292) |
| 531.8(2) | 13(3) | *N* | | | | | | | | |
| 539.1(2) | 52(4) | *N* | 6.5(8) | $M1,(E2)$ | (60) | 104 | 133 | 296 | | |
| 551.6(5) | 19(4) | *N* | | | 69 | 104 | 133 | 167 | 198 | (237) |
| 553.9(1) | 47(5) | *N* | | | 350 | 373 | | | | |
| 569.05(9) | 35(2) | *N* | 6.2(7) | $M1$ | 104 | | | | | |
| 584.0(4) | 57(6) | | 5.7(7) | $M1$ | 60 | 104 | 133 | 296 | (257) | |
| 598.3(3) | 31(3) | | | | 350 | 373 | | | | |
| 609.5(1) | 32(14) | *N* | 3.4(9) | $E2$ | 69 | 104 | 133 | 167 | 198 | 237 |
| 637.2(1) | 61(4) | *N* | | | 104 | 167 | | | | |
| 641.2(2) | 5(2) | *N* | | | 104 | 167 | | | | |
| 661.2(4) | 21(4) | *N* | | | 69 | 104 | 133 | 167 | (198) | |
| 653.8(2) | 14(3) | *N* | | | | | | | | |
| 672.7(1) | 33(4) | *N* | | | | | | | | |
| 684.6(3) | 14(2) | *N* | | | 104 | | | | | |
| 696.4(1) | 17(4) | *N* | 3.1(3) | $M1,E2$ | 104 | 133 | 159 | 167 | 229 | (292) |
| | | | | | 358 | | | | | |
| 703.8(3) | 16(5) | *N* | 3.1(3) | | 104 | 122 | 167 | | | |
| 704.3(2) | 53(6) | *N* | | | | | | | | |
| 719.9(3) | 14(2) | *N* | | | | | | | | |
| 731.0(5) | 15(2) | *N* | | | (104) | (167) | | | | |
| 742.58(4) | 158(12) | | 4.0(10) | $M1$ | | | | | | |
| 749.89(5) | 69(4) | *N* | 3.2(6) | $M1$ | | | | | | |
| 768.5(2) | 64(7) | *N* | 2.5(3) | $M1,E2$ | 104 | | | | | |
| 770.14(8) | 39(8) | *N* | | | | | | | | |
| 788.1(1) | 31(4) | *N* | | | | | | | | |
| 793.7(4) | 68(2) | *N* | 3.2(7) | $M1$ | 104 | | | | | |
| 797.16(4) | 125(18) | | 3.1(8) | $M1$ | | | | | | |
| 804.6(3) | 52(7) | *N* | | | | | | | | |
| 808.17(4) | 67(15) | | 2.7(4) | $M1$ | 122 | | | | | |
| 820.98(4) | 133(14) | | 1.9(2) | $E2$ | | | | | | |
| 841.1(2) | 29(9) | *N* | | | 104 | 167 | | | | |
| 842.4(5) | 56(6) | *N* | | | | | | | | |
| 846.4(5) | 49(4) | *N* | | | | | | | | |
| 864.2(3) | 21(3) | *N* | | | 104 | | | | | |
| 870.8(5) | 10(2) | *N* | | | | | | | | |
| 874.4(2) | 21(7) | *N* | | | 104 | | | | | |
| 880.6(5) | 17(2) | | | | | | | | | |
| 897.7(1) | 35(2) | *N* | | | | | | | | |
| 904.5(3) | 32(3) | *N* | | | | | | | | |
| 924.5(5) | 53(7) | *N* | | | | | | | | |
| 933.6(3) | 100(10) | *N* | | | | | | | | |
| 968.1(1) | 46(5) | *N* | | | | | | | | |
| 970.7(1) | 41(4) | | | | | | | | | |

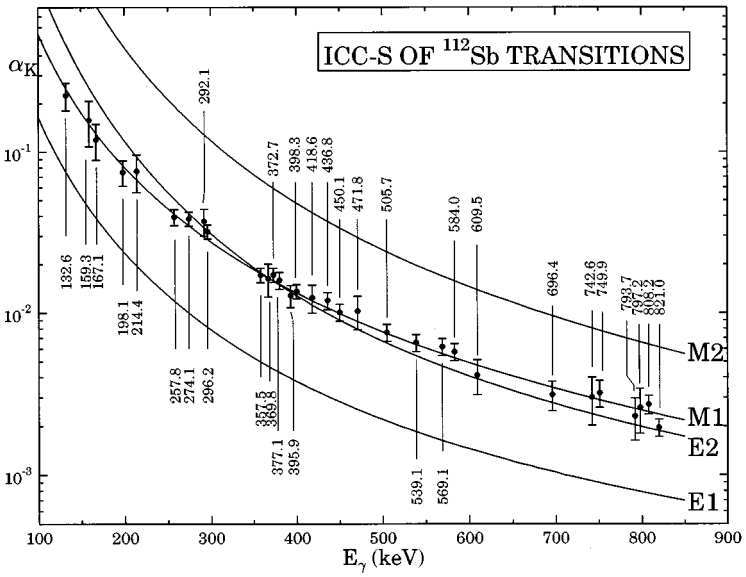


FIG. 3. The internal conversion coefficients of $^{112}$Sb transitions.

present work on the basis of their coincidence relations. Typical $\gamma\gamma$-coincidence spectra are shown in Fig. 2. The energies and relative intensities of $\gamma$ rays are listed in Table I, together with their internal conversion coefficients, multipolarities, and coincidence relations.

The internal conversion coefficients (ICC's) of more than 30 $^{112}$Sb transitions were determined, all of them are new. It is worth noting that each transition has $M1/E2$ multipolarity. The ICC's obtained are shown in Fig. 3.

The results of the angular distribution measurements are summarized in Table II. The reduced $\chi^2$ fits of the theoretical distributions to the experimental ones are shown in Fig. 4. In general, only spin, parity, and multipole-mixing-ratio values allowed by the internal conversion coefficient measurements were considered in the angular-distribution fits. Spins were rejected on the basis of a 0.1% confidence limit. The uncertainty of the mixing ratios ($\delta$) corresponds to the $\chi^2_{\min}+1$ values. All the $\gamma$ lines for which the angular distribution could be measured are of $\Delta I=0$ or $\Delta I=1$ nature. For about one-third of them the $\Delta I=0$ possibility could also be excluded. For every $\gamma$ ray $\delta\sim 0$ was found.

## IV. LEVEL SCHEME OF $^{112}$Sb

The level scheme obtained from the $^{112}$Sn$(p,n\gamma)$ reaction was constructed mainly from $\gamma\gamma$-coincidence results, but the energy and intensity balances of transitions were also taken into account. The proposed level scheme up to 810 keV is displayed in Fig. 5.

The proposed level scheme contains five excited states below 170 keV. Two of them at 61.0 and 129.6 keV are new. The existence of the new level at 129.6 keV was deduced from the fact, among others that the strong transitions of 167.1 and 103.8 keV, which are not in coincidence with each other, were seen in several gates with a constant intensity ratio. Both of them are connected to the ground state, and there are several pairs of $\gamma$ rays with 63.3 keV energy difference decaying from the same level, which are in coincidence with the 103.8 and 167.1 keV transitions, respectively, establishing this placement. On the other hand, there is no 63.3 keV transition in the appropriate gate spectra which could connect the two states. Thus, for the connection of the 103.8 and 167.1 keV levels assumption of a cascade of low-energy transitions was necessary. As the connecting transitions must be strong enough, in spite of the internal conversion they are expected to be visible in the LEPS spectra down to $\sim$30 keV. A 37.5 keV transition was found, which is well distinguished from the 38.3 keV $^{112}$Sb transition in the LEPS spectra, and which could be assigned to the $^{112}$Sb on the basis of the intensity ratios obtained, when targets with different enrichments were used. There is a peak in the spectrum also at $\sim$26 keV, needed to cover the 63.3 keV energy difference, but it corresponds mainly to the Sn x rays, and the existence of a $\gamma$ ray of this energy cannot be directly proved. On the other hand, this was the only possible combination for bridging the energy and intensity gaps between the 167.1 and 103.8 keV states.

The strong 350.0 and 372.7 keV transitions were also observed in several gates with constant intensity ratios, which suggest that either they originate from the same state, or there is a low-energy 22.7 keV transition hidden under the low-energy tail of the Sn, Sb x rays, which connects the levels they decay from. Both the $\beta$ decay [5] and the in-beam [6] studies suggest that the 372.7 keV transition originates from a $1^+$ state. As the low feeding of an independent 350 keV state would lead to spin 4,5 for it [6], the existence of a low-energy transition between the spin 1 and 4 states can be excluded. Thus the two transitions must originate from the same level. For the decay of the state populated by the 350.0 keV $\gamma$ ray a 22.7 keV transition is to be assumed. Since the initial state of the 372.7 keV transition has spin parity $1^+$, and the ground state has $3^+$, the 372.7 keV transition should be a stretched $E2$ transition, which is excluded by our angular distribution measurement. To avoid this conflict the 372.7 keV transition was placed feeding the 38 keV state. This placement leads to the new 61.0 keV state. In addition to the 350 keV transition several other gamma rays placed on the basis of energy and intensity balances populate this state confirming its existence.

After solving these problems the construction of the level

TABLE II. Results of the gamma ray angular distribution measurements from the $^{112}$Sn$(p,n\gamma)^{112}$Sb reaction performed at $E_p=9.3$ MeV. Delta values are marked by an asterisk, if the spin combination is rejected due to high $\chi^2$ value, or the mixing ratio ($\delta$) obtained for a stretched E2 transition is a finite value within its uncertainty. The uncertainty of the mixing ratio is given for the accepted spin combination.

| | | | | $\gamma$-ray angular distribution measurements | | | | | |
|---|---|---|---|---|---|---|---|---|---|
| $E_i$ (keV) | $E_f$ (keV) | $E_\gamma$ (keV) | Multip. | $A_2$ | $A_4$ | $J_i$ Supposed | $J_f$ | $\delta$ | $J_{i/f}$ Adopted[a] |
| 103.8 | 0.0 | 103.8 | | −0.264(86) | −0.042(73) | $1^+$ | $3^+$ | * | |
| | | | | | | $2^+$ | | +0.39 | |
| | | | | | | $3^+$ | | −1.77 | |
| | | | | | | $4^+$ | | −0.01(4) | $4^+$ |
| | | | | | | $5^+$ | | * | |
| 167.1 | 0.0 | 167.1 | $M1$ | −0.254(95) | −0.044(81) | $2^+$ | $3^+$ | +0.35 | |
| | | | | | | $3^+$ | | −1.57 | |
| | | | | | | $4^+$ | | +0.01(4) | $4^+$ |
| 236.4 | 167.1 | 69.4 | | −0.145(103) | −0.132(89) | $2^+$ | $4^+$ | * | |
| | | | | | | $3^+$ | | +0.02(8) | 3 |
| | | | | | | $4^+$ | | −0.77 | |
| | | | | | | $5^+$ | | +0.11 | |
| | | | | | | $6^+$ | | * | |
| | 103.8 | 132.6 | $M1$ | −0.011(107) | 0.064(93) | $3^+$ | $2^+$ | +0.16 | |
| | | | | | | | $3^+$ | −0.52 | |
| | | | | | | | $4^+$ | −0.07(6) | $4^+$ |
| | 38.3 | 198.1 | $M1$ | −0.243(139) | −0.133(121) | $3^+$ | $2^+$ | −0.04(6) | $2^+$ |
| | | | | | | | $3^+$ | * | |
| | | | | | | | $4^+$ | −0.09 | |
| 296.2 | 0.0 | 296.2 | $M1,E2$ | −0.006(31) | −0.036(26) | $1^+$ | $3^+$ | * | |
| | | | | | | $2^+$ | | −0.07(4) | $2^+$ |
| | | | | | | $3^+$ | | −0.48 | |
| | | | | | | $4^+$ | | −0.15 | |
| | | | | | | $5^+$ | | * | |
| 395.9 | 38.3 | 357.5 | $M1,E2$ | −0.234(105) | −0.024(89) | $3^+$ | $1^+$ | * | |
| | | | | | | | $2^+$ | +0.01(5) | $2^+$ |
| | | | | | | | $3^+$ | +0.08 | |
| | | | | | | | $4^+$ | +0.13 | |
| | | | | | | | $5^+$ | * | |
| | 103.8 | 292.1 | $M1,E2$ | −0.154(132) | 0.017(111) | $3^+$ | $1^+$ | * | |
| | | | | | | | $2^+$ | +0.05 | |
| | | | | | | | $3^+$ | −0.85 | |
| | | | | | | | $4^+$ | +0.07(9) | $4^+$ |
| | | | | | | | $5^+$ | * | |
| 411.1 | 38.3 | 372.7 | $M1,E2$ | −0.002(81) | −0.001(71) | $1^+$ | $0^+$ | * | |
| | | | | | | | $1^+$ | −0.17 | |
| | | | | | | | $2^+$ | −0.07(4) | $2^+$ |
| | | | | | | | $3^+$ | +0.13 | |
| 502.1 | 167.1 | 335.1 | $M1,E2$ | −0.229(371) | −0.058(311) | $5^+$ | $3^+$ | * | |
| | | | | | | | $4^+$ | −0.14(8) | $4^+$ |
| | | | | | | | $5^+$ | −0.36 | |
| | | | | | | | $6^+$ | +0.26 | |
| | | | | | | | $7^+$ | * | |
| | 103.8 | 398.3 | $M1,E2$ | −0.508(218) | −0.010(169) | $2^+$ | $4^+$ | * | |
| | | | | | | $3^+$ | | +0.47 | |
| | | | | | | $4^+$ | | −1.92 | |
| | | | | | | $5^+$ | | −0.14(8) | $5^+$ |
| | | | | | | $6^+$ | | * | |
| 510.7 | 395.9 | 114.9 | | −0.147(135) | −0.077(116) | $1^+$ | $3^+$ | * | |
| | | | | | | $2^+$ | | +0.07(15) | $2^+$ |

TABLE II. (*Continued*).

| | | | | $\gamma$-ray angular distribution measurements | | | | | |
|---|---|---|---|---|---|---|---|---|---|
| $E_i$ (keV) | $E_f$ (keV) | $E_\gamma$ (keV) | Multip. | $A_2$ | $A_4$ | $J_i$ Supposed | $J_f$ | $\delta$ | $J_{i/f}$ Adopted[a] |
| | | | | | | $3^+$ | $-0.69$ | | |
| | | | | | | $4^+$ | $+0.10$ | | |
| | | | | | | $5^+$ | * | | |
| | 236.4 | 274.1 | $M1,E2$ | $-0.276(166)$ | $-0.176(146)$ | $1^+$ | $3^+$ | * | |
| | | | | | | $2^+$ | $+0.19(17)$ | $2^+$ | |
| | | | | | | $3^+$ | $-1.02$ | | |
| | | | | | | $4^+$ | $+0.06$ | | |
| | | | | | | $5^+$ | * | | |
| 714.8 | 296.2 | 418.6 | $M1,E2$ | $-0.057(100)$ | $-0.004(87)$ | 0 | $2^+$ | $\infty$ | |
| | | | | | | $1^+$ | $+0.28(56)$ | $(1)^+$ | |
| | | | | | | $2^+$ | $-0.43$ | | |
| | | | | | | $3^+$ | $+0.14$ | | |
| | | | | | | $4^+$ | * | | |
| 780.9 | 411.1 | 369.8 | $(M1,E2)$ | $-0.304(219)$ | $-0.104(183)$ | $1^+$ | $1^+$ | $-1.0$ | |
| | | | | | | 0 | * | | |
| | | | | | | $2^+$ | $-0.02(14)$ | $2^+$ | |
| | | | | | | $3^+$ | * | | |
| 808.2 | 0.0 | 808.2 | $M1$ | 0.022(396) | $-0.179(342)$ | $2^+$ | $3^+$ | $-0.33(27)$ | |
| | | | | | | $3^+$ | | $-0.28(25)$ | |
| | | | | | | $4^+$ | | $+0.25(11)$ | $4^+$ |

[a]Based on all available data.

scheme was self-evident. The only questionable placement remained was that of the 236.7 keV transition. It is in coincidence with the 103.8 keV $\gamma$ ray that can be fulfilled either by putting the transition onto the 103.8 or the 129.6 keV states. After the spin determination this transition was placed to decay into the new 129.6 keV state, else the initial state of the transition would have spin 6 the final one spin 4, leading to a low-energy stretched $E2$ transition, which is extremely rare between low spin states of odd-odd Sb nuclei.

Comparing our level scheme to that obtained from $\beta$ decay [5], it can be concluded that the levels at 38, 104, 236, 296, and 715 keV are in agreement, but the 372 and 350 keV $\gamma$ rays representing two different levels were assigned as decays from the 411 keV level on the basis of their coincidence relations and the above discussion.

The levels at 104, 167, 236, 296, 395, 501, and 715 keV of the in-beam study [6] are in agreement with our results. The 372 and 236 keV gamma rays were assigned to higher energy levels as explained above, as well as the 357 keV gamma ray on the basis of its coincidence relations.

Apart from the levels obtained by replacing previously known gamma rays, our level scheme contains four new levels even below 715 keV, the energy region where our investigations overlap with the previous ones, and there are about four times as many transitions in it as in the earlier works. All the higher energy states are new.

### A. Hauser-Feshbach analysis

As all but a few very weak lines assigned to $^{112}$Sb are placed in the level scheme, the level scheme obtained for this nucleus can be considered nearly complete, thus the cross sections for the neutron groups feeding the different levels can be deduced from the transition intensities.

The $\sigma_{\rm lev}(p,n)$ relative cross sections obtained in this way are shown in Fig. 6 for different bombarding proton energies. The internal conversion coefficients of the $\gamma$ rays deexciting the levels below 150 keV are not known, and due to the low energy of these transitions, the majority of the transition intensities is furnished by conversion processes. Consequently, the neutron cross sections for these levels cannot be deduced precisely enough from the $\gamma$-ray intensities, so the levels below 150 keV were ignored from the analysis.

Hauser-Feshbach theoretical results have been calculated with the CINDY [13] program, which is based on the compound reaction model. The transmission coefficients were calculated using the optical model parameter set of Wilmore and Hodgson [15] for neutrons and that of Perey [16] (modified by Gyarmati *et al.* [17]) for protons. The parameters of the optical potentials are given in Table III. Beside the neutron channels, some $(p,p')$ channels were also included. The experimental and theoretical cross sections were normalized at the 411.1-keV $1^+$ state. In calculations of the theoretical curves, the values of the cross sections are interdependent, since changing the spin of any individual level requires the redistribution of the outgoing flux through all the other channels. Nevertheless, the variation of the spin and parity of one level can cause only 5–10 % change in the cross sections of the others. This means that using only the Hauser-Feshbach analysis we cannot make distinction between spins 1 and 3, nor between 0 and 4, and the analysis is not sensitive to the parity.

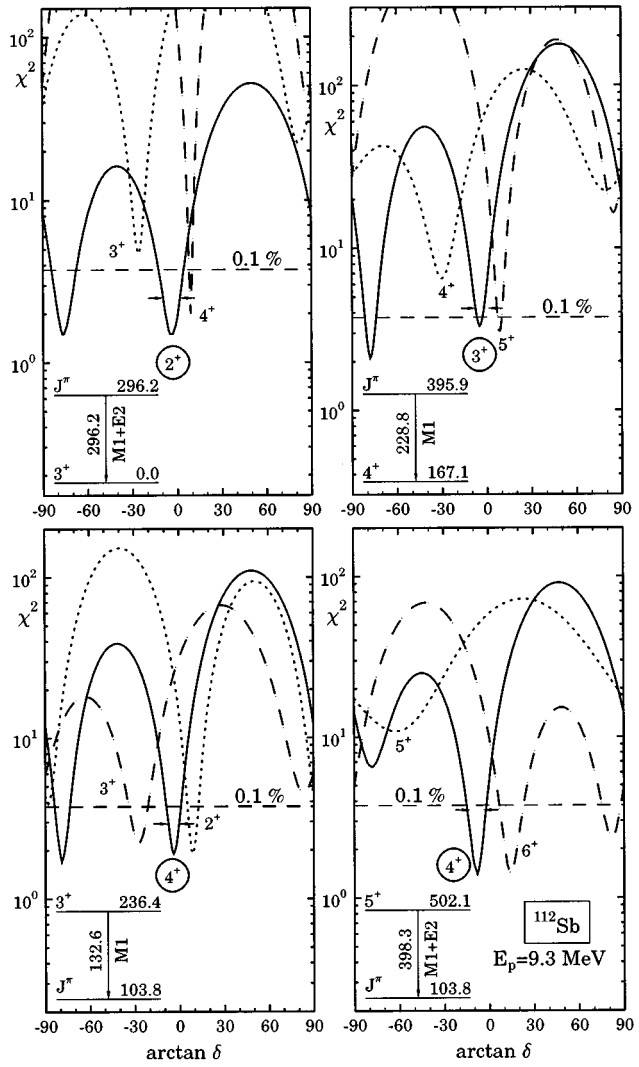


FIG. 4. The reduced $\chi^2$ fits of the theoretical angular distributions of $\gamma$ rays to the experimental ones as a function of arctan$\delta$, where $\delta^2$ is the $E2/M1$ intensity ratio for the transition. Labeling numbers are the assumed spins and parities for the state in question. Encircled numbers are adopted spins and parities based on all available data. The dashed lines show the 0.1% confidence limit for the reduced $\chi^2$.

### B. Spin and parity assignment

The level spin assignments are based on the measured internal conversion coefficients of transitions, on the Hauser-Feshbach analysis, and on the $\gamma$-ray angular distribution results. The parities came exclusively from the multipolarity measurement.

We used a multistep approach to assign spin and parity values to the levels. In the first step we determined the spins and parities of higher lying states. Using then the multipolarity and angular distribution data for transitions from these higher lying states we could determine the spins and parities of the low lying states, too.

For states above 150 keV the spin values were determined first of all from the Hauser-Fesbach analysis, the dichotomy between spin 1 and 3 or 0 and 4 values were resolved using the multipolarity and angular distribution data.

In the case of the 510.7 keV state the feeding of the state could be determined only with large error, leading to spin range 1 to 3 for this state. The angular distribution of the 114.9 and 274.1 keV transitions feeding $3^+$ states allowed spin 2, 3, or 4, which limited the possible spin range to 2 or 3 for this state.

In the case of the 714.8 keV state both the angular distribution and the Hauser-Feshbach analysis allowed spin 1 and 3 values. The spin 3 value was excluded on the basis of the log$ft$ value from the $\beta$ decay work [5].

For the spin determination of the 38.3 and 103.8 keV states the angular distribution data and the spin values obtained for the higher lying states were used. The 38.3 keV state is fed by an $M1$ transition from the 296 keV $2^+$ state, a $\Delta I=1$ transition from the 236 keV $3^+$ state, and a $\Delta I=0,1$ transition from the 411 keV $1^+$ state. The only spin parity value allowed by these requirements is $2^+$.

The 103.8 keV state is populated via $\Delta I=0,1$ transitions from the 395.9 keV $3^+$, the 236.4 keV $3^+$, and the 502.1 keV $5^+$ states, allowing only for the $4^+$ spin assignment.

The 61 keV state is fed by transitions from $1^+$ states and by an $M1$ transition from the 781 keV $2^+$ state, making the 1, 2, and $3\hbar$ spin assignments possible. The 129.6 keV state is connected to $4^+$ states via low-energy, probably dipole transitions, which suggests spin 3, 4, or 5 for this state. One can also consider that these states do not decay to the $3^+$ ground state, although a ground state transitions would be enhanced by a factor of 20 for the 61 keV, and a factor of 140 for the 129.6 keV state according to the $E_\gamma^3$ scaling for dipole transitions. The lack of such transitions suggest that the spin of these states differ by $2\hbar$ units from that of the ground state. As the missing of the transitions may also be a result of some strong selection rule, the $1^+$ and 5 spin values are only tentative assignments to the 61 and 129.6 keV states, respectively.

Our spin values are in agreement with that of the work of Kamermans *et al.* [6] taking into account the replacement of the gamma rays, except for the 395.9 keV level, which is a $3^+$ in our level scheme, compared to the spin 5 of Ref. [6]. A possible reason for this discrepancy may be that we observed more $\gamma$ transitions deexciting this state, which resulted in higher excitation cross section, giving a lower spin value. Our assignments differ at one point also from that of Ref. [5]. We have deduced spin 2 for the 38.3 keV state instead of 1, and the spin 1 state is at 61.0 keV. The spin 1 value was deduced from the intensity of the 38 keV transition, serving as the basis for determination of the log$ft$ value. As the 61.0 keV state is decaying 100% to the 38.3 keV state, it is expected that the 38.3 keV transition will have the same intensity in the decay of $^{112}$Te, in spite of the fact that it is populating now mainly the 61.0 keV state.

## V. PROTON-NEUTRON MULTIPLET STATES

In an odd-odd nucleus the excited states are expected to arise from the angular momentum coupling of the different proton and neutron states. In zeroth-order approximation the energy of the $p$-$n$ multiplet can be obtained by addition of energies of the odd proton and odd neutron states. The multiplets are split by the effective proton-neutron interaction.

The low lying states of the neighboring $^{111}_{51}$Sb and

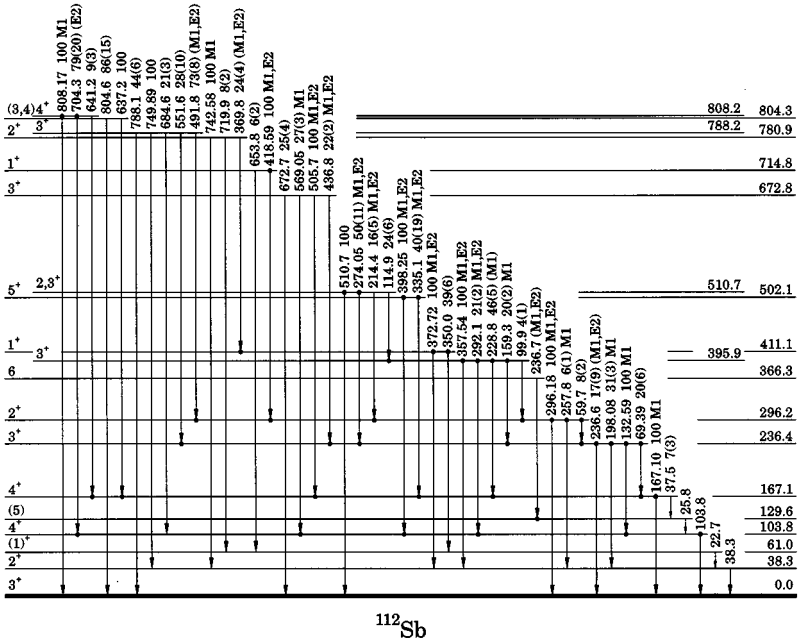


FIG. 5. Proposed level scheme of $^{112}$Sb from the $(p,n\gamma)$ reaction. Solid circles at the ends of arrows indicate $\gamma\gamma$-coincidence relations. $\gamma$-branching ratios and multipolarities are also given. The 22.7 and 25.8 keV transitions were not observed, their energy values have been inferred.

$^{111}\mathrm{Sn}_{61}$ [18] are shown in Fig. 7(a). Below 850 keV there is only the $5/2^+$ ground state of $^{111}$Sb, which is expected to have dominant $\pi d_{5/2}$ configuration. The low lying states of $^{111}$Sn with $7/2^+$, $5/2^+$, $1/2^+$, $3/2^+$, and $5/2^+$ at 0, 155, 255, 643, and 755 keV excitation energies have $\nu g_{7/2}$, $\nu d_{5/2}$, $\nu s_{1/2}$, $\nu d_{3/2}$, and $\nu g_{7/2}\oplus 2^+$ character, respectively [19].

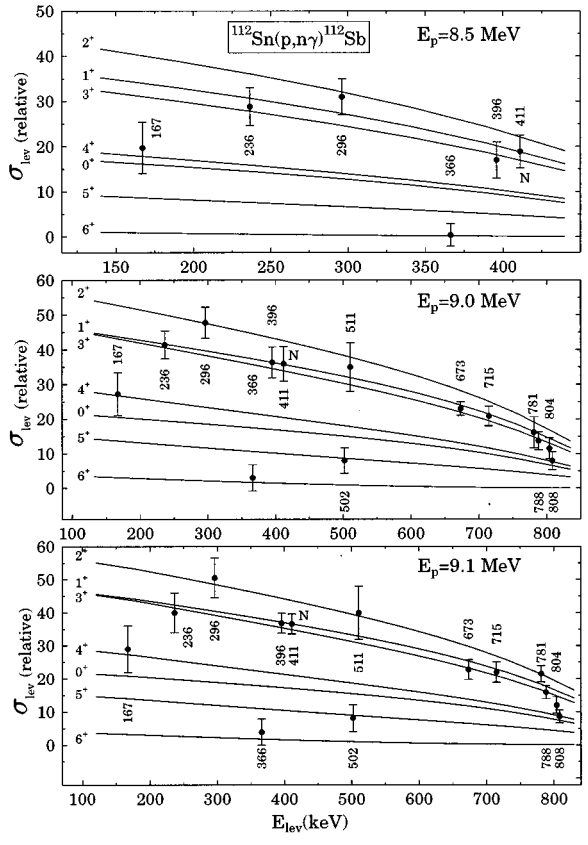


FIG. 6. Experimental relative cross sections ($\sigma_{\mathrm{lev}}$) of the $^{112}\mathrm{Sn}(p,n\gamma)^{112}\mathrm{Sb}$ reaction as a function of the level energy ($E_{\mathrm{lev}}$) at 8.5 and 9.0 MeV bombarding proton energies. The solid and dashed curves show Hauser-Feshbach theoretical results.

According to Fig. 7(a), the lowest lying states of $^{112}$Sb are expected to be members of the proton-neutron multiplets based on the $\pi d_{5/2}$ proton configuration. To estimate the splitting of the different multiplets we carried out a parabolic rule [20] calculation. The calculations were performed in a way similar to those for $^{112}$In [21], using the same formulas.

The parameters of the calculations were the strength of the quadrupole core polarization interaction $\alpha_2^0=4.2$ MeV and the strength of the spin polarization interaction, $\alpha_1^0\sim 15/A=0.13$ MeV. These values are the same as used for the interpretation of $^{114}$Sb and are very close to those used in the description of the structure of $^{118}$Sb [4]. The occupation probabilities of quasineutron states were calculated in BCS approximation using the single-particle energies and pairing interaction strength of Kisslinger and Sorensen [22]. They are as follows: $V^2(\nu d_{3/2})=0.07$, $V^2(\nu d_{5/2})=0.76$, $V^2(\nu g_{7/2})=0.56$, and $V^2(\nu s_{1/2})=0.29$.

The result of the calculations are presented in Fig. 7(b). As in the case of other parabolic rule calculations, we used one overall normalization term, which pushed up all the members of the multiplets by the same energy.

The levels determined from our measurements are presented in Fig. 7(c). The experimental states could be associated with the calculated ones on account of energies, spins, and dominant decay modes, since in quasiparticle shell model strong ($\sim$1 Weisskopf unit) $M1$ transitions are expected between the $J$ and $J\pm 1$ members of the multiplets. The dominant decay mode was determined by rescaling the branching ratios of the transitions with $E_\gamma^3$. For states above 200 keV, where branching takes places at all, this rescaling leads to a very prominent selection. The main branch is 10–50 times stronger than the side branches.

*The $\pi d_{5/2}\nu g_{7/2}$ multiplet.* The ground state is expected to arise from the $\pi d_{5/2}\nu g_{7/2}$ configuration in analogy with the neighboring $^{114}$Sb nucleus. On the low spin side the 23–38-keV $\gamma$ cascade decays into the ground state, indicating that the 61-keV $1^+$ and the 38-keV $2^+$ states are the $1^+$ and $2^+$

TABLE III. Optical model parameters used in this work. The V, W, and $V_{so}$ potential depths are given in MeV and the $r$ range and $a$ diffuseness parameters are in fm. $E$ is the energy of the bombarding proton or outgoing neutron, given in MeV.

| | $V$ | $W$ | $V_{so}$ | $r_{real}$ | $r_{imag.}$ | $a_{real}$ | $a_{imag.}$ |
|---|---|---|---|---|---|---|---|
| $p+^{112}$Sn[a] | 60.34-0.55$E$ | 13.5 | 7.5 | 1.25 | 1.25 | 0.65 | 0.47 |
| $n+^{112}$Sb[b] | 47.01-0.267$E$- -0.0018$E^2$ | 9.52- -0.053$E$ | 7.0 | 1.28 | 1.24 | 0.66 | 0.48 |

[a]From Ref. [16].
[b]From Ref. [15].

members of the ground state multiplet. On the high spin side the ground state is favored by the 236–26–104-keV cascade, suggesting that the 366-keV 6, the 130-keV 5, and the 104-keV $4^+$ states form the high spin part of the multiplet. The parabolic rule predicts a nearly degenerate multiplet, as the quasiparticle blocking factor $(U^2-V^2)$ makes practically ineffective the quadrupole-quadrupole component of the effective interaction. The members of the multiplet have energies less than 130 keV, only the possible $6^+$ member seems to be somewhat higher in energy.

*The $\pi d_{5/2}\nu d_{5/2}$ multiplet.* This multiplet is a particle-hole multiplet, having an open up parabolic shape. The 419–60-keV cascade selects the 715 keV $1^+$, 296 keV $2^+$, and 236 keV $3^+$ states to belong to the same multiplet. Although the dominant decay mode of this state leads to the 167 keV $4^+$ state, assigning this state also to the $\pi d_{5/2}\nu d_{5/2}$ multiplet, it is only a factor of 3 stronger than the transition to the 104 keV $4^+$ state. The situation is even worse for the case of the 502-keV $5^+$ state, which may be the $5^+$ member of the multiplet. These branchings suggest that the two $4^+$ states are mixed. This assumption is in agreement with the decay of the 104-keV state, but not with that of the 167-keV one. It should then decay via a 63 keV transition to the 104-keV state, which might be possible, if this transition is weak enough, but it should also decay via allowed $M1$ transition to the ground state. The $B(M1)$ value of the 167 keV transition is, on the other hand, only a few percent of the 37.5 keV transition allowing only a few percent mixing instead of the few times ten percent expected from the decay of the 236 and 502 keV states.

*The $\pi d_{5/2}\nu s_{1/2}$ multiplet.* This doublet of $2^+$ and $3^+$ states may correspond to the 510-keV $2,3^+$ and the 396-keV $3^+$ states, which are selected to belong to the same multiplet by the 115 keV transition. The 296 keV state decays to the lower lying ones with intensities of the same order of magnitude, in agreement with the expectations.

*The $\pi d_{5/2}\nu d_{3/2}$ multiplet.* Although the centroid of this multiplet is expected to lie at a relatively high energy, because of the strong splitting, as well as the attractive $\pi d_{5/2}-\nu d_{3/2}$ interaction, some states of this multiplet may intrude to observable energies. The 411-keV $1^+$ state and the 781-keV $2^+$ one were assigned to this multiplet, which are connected via the 370 keV transition. There is a relatively strong branch from this state to the 38 keV one, which indicates that this state may also contain significant one-phonon component. The $3^+$ member of this multiplet is predicted to lie above 1 MeV. The states at 804 and 808 might be candidates for the $4^+$ member of the multiplet.

Up to 780 keV all states but one were identified as a quasiparticle state, using the parabolic rule. The unidentified state might arise either from the one-phonon states or from $\pi g_{7/2}$ configuration based multiplets.

Comparing the energies obtained from the parabolic rule with those from the number-projected quasiparticle calculations of Gunsteren *et al.* [8] shown in Fig. 7(d), it is seen that the calculated shapes are quite different. The $\pi d_{5/2}\nu g_{7/2}$ multiplet has open-up, while the $\pi d_{5/2}\nu d_{5/2}$ and the $\pi d_{5/2}\nu d_{3/2}$

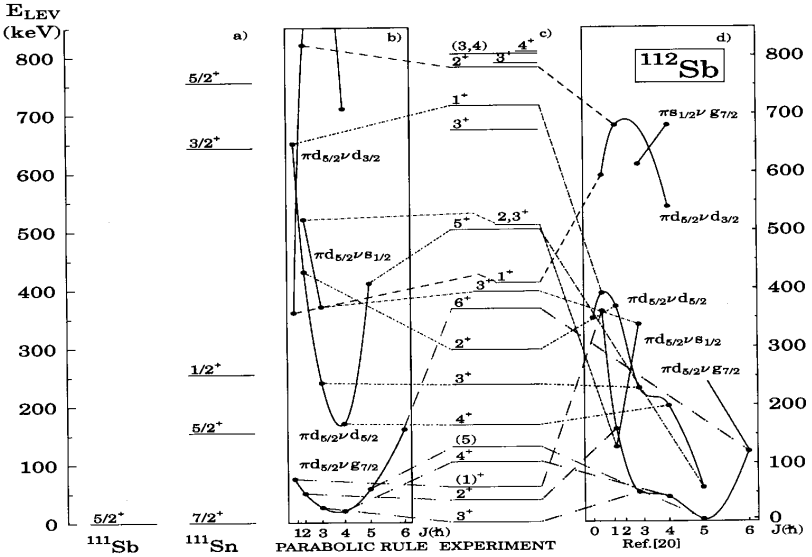


FIG. 7. Proton-neutron multiplet states in $^{112}$Sb. (a) Experimental level energies and configurations of the lowest lying states of $^{111}$Sb and $^{111}$Sn. (b) Results of the parabolic-rule calculations for positive parity states. The abscissa is scaled according to $J(J+1)$, where $J$ is the spin of the state. (c) Experimental results on $^{112}$Sb levels, (d) results of the calculations by Gunsteren *et al.* [8].

ones have compressed open-down shapes. These differences suggest that in Ref. [8] the occupation probabilities of the neutron states were different from the values that we used in our calculations. The deviation of the splitting of the $\pi d_{5/2}\nu g_{7/2}$ multiplet from the parabolic shape is a consequence of the use of short range effective interaction in Ref. [8].

**ACKNOWLEDGMENTS**

We are indebted to Professor Dr. T. Fényes for useful discussions. The assistance in experiments of the cyclotron staff, as well as of the members of the cryogenic laboratory, is recognized. We are indebted also to Dr. S. Mészáros and Dr. A. Valek for their help in the measurements.

[1] Z. Gácsi and Zs. Dombrádi, Phys. Rev. C **50**, 1833 (1994).
[2] Z. Gácsi, T. Fényes, and Zs. Dombrádi, Phys. Rev. C **44**, 626 (1991).
[3] Z. Gácsi, Zs. Dombrádi, T. Fényes, S. Brant, and V. Paar, Phys. Rev. C **44**, 642 (1991).
[4] J. Gulyás, T. Fényes, M. Fayez Hassan, Zs. Dombrádi, J. Kumpulainen, and R. Julin, Phys. Rev. C **46**, 1218 (1992).
[5] M. E. J. Wigmans, R. J. Heynis, P. M. A. van der Kam, and H. Verheul, Phys. Rev. C **14**, 243 (1976).
[6] R. Kamermans, H. W. Jongsma, T. J. Ketel, R. van der Wey, and H. Verheul, Nucl. Phys. **A266**, 346 (1976).
[7] K. Miyano and C. Gil, J. Phys. Soc. Jpn. **33**, 1509 (1972).
[8] W. F. van Gunsteren, K. Allart, and E. Boeker, Nucl. Phys. **A266**, 365 (1976).
[9] Z. Árvay, T. Fényes, K. Füle, T. Kibédi, S. László, Z. Máté, Gy. Mórik, D. Novák, and F. Tárkányi, Nucl. Instrum. Methods **178**, 85 (1980); T. Kibédi, Z. Gácsi, A. Krasznahorkay, and S. Nagy, *ATOMKI Annual Report* (ATOMKI, Debrecen, 1986), p. 55; T. Kibédi, Z. Gácsi, and A. Krasznahorkay, *ibid.* p. 100.
[10] J. Blachot and G. Marguier, Nucl. Data Sheets **59**, 333 (1990).
[11] J. Lyttkeis, K. Wilson, and L. P. Ekström, Nucl. Data Sheets **33**, 1 (1981).
[12] H. Helppi, University of Jyväskylä, JYFL Report 1/1976.
[13] E. Sheldon and V. C. Rogers, Comput. Phys. Commun. **6**, 99 (1973).
[14] G. Székely, Comput. Phys. Commun. **34**, 313 (1985).
[15] D. Wilmore and P. E. Hodgson, Nucl. Phys. **55**, 673 (1964).
[16] F. G. Perey, Phys. Rev. **131**, 745 (1963).
[17] B. Gyarmati, T. Vertse, L. Zolnai, A. I. Barishnikov, A. F. Gurbich, N. N. Titarenko, and E. L. Yadrovsky, J. Phys. G **5**, 1225 (1979).
[18] I. Blachot and F. Haas, Nucl. Data Sheets **60**, 889 (1990).
[19] P. J. Blankert, H. P. Blok, and J. Blok, Nucl. Phys. **A36**, 74 (1981).
[20] V. Paar, Nucl. Phys. **A331**, 16 (1979).
[21] T. Kibédi, Zs. Dombrádi, T. Fényes, A. Krasznahorkay, J. Tímár, Z. Gácsi, A. Passoja, V. Paar, and D. Vretenar, Phys. Rev. C **37**, 2391 (1988).
[22] L. S. Kisslinger and R. A. Sorensen, Rev. Mod. Phys. **35**, 853 (1963).